Size-resolved and chemically resolved model of atmospheric aerosol dynamics

Zhaoyue Meng

Department of Environmental Engineering Science, California Institute of Technology, Pasadena

Donald Dabdub

Department of Mechanical and Aerospace Engineering, University of California at Irvine

John H. Seinfeld

Division of Engineering and Applied Science and Department of Chemical Engineering, California Institute of Technology, Pasadena

Abstract. A three-dimensional, size-resolved and chemically resolved aerosol model is developed. Gas-to-particle conversion is represented by dynamic mass transfer between the gas and aerosol phases. Particle-phase thermodynamics is computed by a new thermodynamic model, Simulating Composition of Atmospheric Particles at Equilibrium 2. The aerosol model is applied to simulate gas and aerosol behavior in the August 27-29, 1987, episode in the South Coast Air Basin of California. The assumption that volatile inorganic species such as NH₄NO₃ are at instantaneous, local equilibrium is examined.

1. Introduction

Particles in the Earth's atmosphere play an important role in atmospheric chemistry, climate, and human health. Atmospheric formation and removal of particles are governed by a number of complex dynamic processes, including nucleation, condensation, coagulation, chemical transformation in the gas, aerosol, and aqueous (cloud and fog) phases, interphase exchange and equilibria, and wet and dry deposition. Atmospheric particle sizes range from a few nanometers (nm) in diameter to several micrometers (µm). This factor of 10³ in diameter translates into a factor of 10⁹ in particle mass between the two extremes of the size spectrum. Particle chemical composition can vary substantially depending on particle size; indeed, this variation is, at once, one of the most important features from the point of view of atmospheric chemistry and human health effects and one of the most demanding aspects to model theoretically.

A gas-phase atmospheric chemical-transport model predicts the spatial and temporal distribution of gaseous species concentrations, $c_i(x, y, z, t), i = 1, 2, ..., N$. An atmospheric aerosol is characterized by both its size and composition distribution. The most general form of an atmospheric aerosol chemical-transport model predicts the size-composition distribution as a function of location and time. The starting point for an aerosol model is the equation of conservation of particle number (or mass). Within that equation are terms that account for transport and dispersion, gas-to-particle conversion, coagulation, and removal processes. *Pilinis and Seinfeld* [1988] constructed the first three-dimensional size-resolved and chemically resolved

Copyright 1998 by the American Geophysical Union.

Paper number 97JD02796. 0148-0227/98/97JD-02796\$09.00

atmospheric aerosol model. The major features of the model, as well as those of some other existing aerosol models, are summarized in Tables 1-4. The first three-dimensional aerosol models assumed instantaneous gas-aerosol equilibrium for volatile inorganic compounds. It has been shown, however, that for some compounds under certain conditions, equilibrium is slow to be established relative to the timescale over which other changes are occurring [Wexler and Seinfeld, 1990; Meng and Seinfeld, 1996]. Thus it is desirable that the most general form of an aerosol model not rely on the assumption of instantaneous, local equilibrium of volatile species.

The models of *Pilinis and Seinfeld* [1988] and *Lurmann et al.* [1997] represent the aerosol size distribution by the sectional approximation [*Gelbard et al.*, 1980; *Gelbard and Seinfeld*, 1980], wherein the size domain is segmented into a series of sections, or bins, within which the aerosol has a uniform composition. The Regional Particulate Matter model [*Binkowski and Shankar*, 1995] assumes that the aerosol size distribution adheres to a bimodal lognormal distribution and then solves equations for the zeroth, third, and sixth moments of the distribution.

We present here the development and application of a threedimensional size-resolved and chemically resolved atmospheric aerosol chemical-transport model. The model is applied to simulate gas and aerosol behavior in the South Coast Air Basin of California over a 3-day episode (August 27-29) during the 1987 Southern California Air Quality Study (SCAQS).

2. Governing Equations for Aerosol Dynamics

Let n(m,t) be the number concentration of particles having total particle mass in the range m to m+dm. (We need not explicitly indicate the spatial dependence of n for the moment.) The total

	Pilinis and Seinfeld [1988]	Lurmann et al. [1997]	Regional Particulate Matter Model	This Work
Overall goal	urban oxidant and aerosol model	urban oxidant and aerosol model	regional particulate model	urban oxidant and aerosol dynamic model
Major applications	Los Angeles Basin	Los Angeles Basin	Eastern United States	Los Angeles Basin
Host air quality model	CIT ^a [McRae et al., 1982; McRae and Seinfeld, 1983]	UAM ^a [Systems Applications International, 1990a, b, c, d, e]	RADM II ^a [Chang et al., 1991]	CIT ^a [Harley et al., 1993]
Meteorological model	constructed through data interpolation with diagnostic wind model	constructed through data interpolation or calculated with land-sea breeze or complex-terrain wind model	PSU/NCAR ^a mesoscale model MM4 [Anthes et al., 1987]	constructed through data interpolation with diagnostic wind model
Gas-phase chemistry	Russell et al. [1988]	SAPRC90 ^a [Carter, 1990]	Stockwell et al. [1990]	extended LCC ^a [Harley et al., 1993]
Horizontal resolution, km	15	4-10	80	5
Vertical resolution	typically five layers to ~1.1 km	typically four layers to ~1.5 km	15 layers to ~100 mb (~15 km)	typically five layers to ~1.1 km
Major references	Pilinis and Seinfeld [1988]	Wexler et al. [1994], and Lurmann et al. [1997]	Binkowski and Shankar [1995]	this paper

^a CIT, California Institute of Technology/Carnegie Institute of Technology; UA, Urban Airshed Model; SAPRC, Statewide Air Pollution Research Center; RADM, Regional Acid Deposition Model; LCC, Lurmann, Carter, Coyner; PSU/NCAR, Pennsylvania State University/National Center for Atmospheric Research.

mass of a particle is the sum of the masses of its N individual components,

$$m = \sum_{i=1}^{N} m_i \tag{1}$$

Let I(m,t) be the rate of change of the total mass of a particle of mass m as a result of condensation/evaporation processes,

$$I(m,t) = \sum_{i=1}^{N} I_{i}(m,t)$$
 (2)

where $I_i = dm_i/dt$. If the coagulation coefficient between particles of masses m and m' is $\beta(m, m')$, the equation of conservation governing n(m, t) can be written as

$$\frac{\partial n(m,t)}{\partial t} = -\frac{\partial}{\partial m} [I(m,t)n(m,t)]
+ \frac{1}{2} \int_{0}^{m} \beta(m',m-m')n(m',t)n(m-m',t)dm'
- n(m,t) \int_{0}^{\infty} \beta(m,m')n(m',t)dm'
+ S(m,t) - L(m,t)n(m,t)$$
(3)

where S(m,t) is any external source of particles of mass m (e.g., nucleation), and L(m,t)n(m,t) is the first-order rate of removal of particles of mass m (e.g., wet and dry deposition).

For applications to urban/regional situations, one is generally interested in the aerosol mass distribution, rather than the number distribution. We define

Table 2. Selected Three-Dimensional, Size-Resolved and Chemically Resolved Aerosol Models: Aerosol Characterization

	Pilinis and Seinfeld [1988]	Lurmann et al. [1997]	Regional Particulate Matter Model	This Work
Number or mass concentration	mass	mass	three moments	mass
Size Resolution, a D_p in μ m	0.05-10 (3)	0.04-10 (8)	two modes (nuclei: 0.01 μm; accumulation: 0.07 μm)	0.04-10 (8)
Multicomponent	yes	yes	yes	yes
Elemental carbon	no	yes	no	yes
Organics Inorganics	yes NH ₃ -H ₂ SO ₄ -HNO ₃ -HCl- Na-H ₂ O	yes NH ₃ -H ₂ SO ₄ -HNO ₃ - HCl-Na-H ₂ O	no NH ₃ -H ₂ SO ₄ -HNO ₃ -H ₂ O	yes NH ₃ -H ₂ SO ₄ -HNO ₃ -HCl- Na-K-Ca-Mg-H ₂ O-CO ₂

The number in parentheses is the typical number of size sections used.

			_	
	Pilinis and Seinfeld [1988]	Lurmann et al. [1997]	Regional Particulate Matter Model	This Work
Nucleation	H ₂ SO ₄ /H ₂ O	H ₂ SO ₄ /H ₂ O	H ₂ SO ₄ /H ₂ O	H ₂ SO ₄ /H ₂ O
Condensation/evaporation	Volatile Inorganics: Gas/particle equilib.; Sulfate+organics: transport	Volatile Inorganics: Gas/particle equilibrium; Sulfate+organics: transport	Volatile Inorganics: Gas/particle equilibrium Sulfate: transport	H ₂ O and CO ₂ : equilibrium; Other compounds: transport
Coagulation	yes	no	yes	no
Dry deposition	Size independent resistance-transfer approach	Size dependent resistance-transfer approach + settling	Mode dependent resistance-transfer approach + settling	Size dependent resistance-transfer approach + settling
Wet deposition	no	no	no	no
Chemical reactions	no	no	no	no
Activation/interaction with fog/cloud	no	no	no	no

Table 3. Selected Three-Dimensional, Size-Resolved and Chemically Resolved Aerosol Models: Aerosol Processes

$$q_i(m,t) = m_i n(m,t) \tag{4}$$

as the mass concentration distribution for species i. The total aerosol mass concentration distribution function is

$$q(m,t) = mn(m,t)$$

$$= \sum_{i=1}^{N} q_{i}(m,t)$$
(5)

The normalized growth/evaporation rate of species i in a particle of mass m is

$$H_i(m,t) = \frac{1}{m} \frac{dm_i}{dt} \tag{6}$$

and the total normalized growth rate of a particle of mass m is

$$H(m,t) = \frac{1}{m} \frac{dm}{dt}$$

$$= \sum_{i=1}^{N} H_{i}(m,t)$$
(7)

Using the above definitions, (3) becomes [Pilinis, 1990]

$$\frac{\partial q_i(m,t)}{\partial t} = H_i(m,t)q(m,t) - \frac{\partial}{\partial m} \left[mq_i H \right]
+ \int_o^m \beta(m',m-m')q_i(m',t) \frac{q(m-m',t)}{m-m'} dm'
- q_i(m,t) \int_o^\infty \beta(m,m') \frac{q(m',t)}{m'} dm'
+ m_i S(m,t) - L(m,t)q_i(m,t)$$
(8)

Table 4. Selected Three-Dimensional, Size-Resolved and Chemically Resolved Aerosol Models: Treatment of Aerosol Thermodynamics

	Pilinis and Seinfeld [1988]	Lurmann et al. [1997]	Regional Particulate Matter Model	This Work
Thermodynamic model	Pilinis and Seinfeld [1987]	Pilinis and Seinfeld [1987]	Saxena et al. [1986]	Kim et al. [1993a, b] Kim and Seinfeld [1995], Meng et al [1995a, b]
Temperature dependence ^a	K	K	K	K and RHD
Binary activity coefficient estimation method ^b	Pitzer	Pitzer	Pitzer	Kusik-Meissner
Multicomponent activity coefficient estimation method	Bromley	Bromley	Bromley	option of Bromley, Kusik-Meissner, and Pitzer
Water activity	ZSR ^c	ZSR	ZSR	ZSR
Organics	No	No	No	formate and acetate

All the models assume chemical equilibrium within the aerosol phase.

^a K and RHD are the equilibrium constant and relative humidity at deliquescence.

^b Binary activity coefficients are not needed for the multicomponent Pitzer method.

^c ZSR, Zdanovskii-Stokes-Robinson.

Equation (8) is the general equation governing the mass distribution of species i over the aerosol mass spectrum. It includes condensation/evaporation, coagulation, sources (such as nucleation), and removal processes. Under the most extreme particle concentrations in urban areas, Brownian coagulation can be shown to have a negligible effect on the evolution of the aerosol size distribution over the timescales of interest [Wexler et al., 1994]. Thus, for urban/regional applications, coagulation can be neglected in (8). The spatial dependence of q can now be accounted for, and terms, identical to those for gaseous species, for advection and turbulent mixing can be added. Finally, for computational purposes the independent variable m can be transformed to a normalized particle diameter $\mu = \ln(D_n/D_{n0})$, where D_{p0} is a reference particle diameter (e.g., the smallest diameter in the size domain). With $p_i(\mu, \mathbf{x}, t) = (dm / d\mu)q_i$, the result is

$$\frac{\partial p_{t}(\mu, \mathbf{x}, t)}{\partial t} = -\left(\overline{V}(\mathbf{x}, t) - V_{s}(\mu)\mathbf{k}\right) \cdot \nabla p_{t} + \nabla \cdot \mathbf{K}(\mathbf{x}, t) \nabla p_{t} + H_{t}(\mu, \mathbf{x}, t) p(\mu, \mathbf{x}, t) - \frac{1}{3} \frac{\partial}{\partial \mu} [H p_{t}] + S_{t}(\mu, \mathbf{x}, t) - L(\mu, \mathbf{x}, t) p_{t} \tag{9}$$

where x is the spatial coordinate vector, $\overline{V}(x,t)$ is the mean wind velocity vector, V_s is the particle settling velocity, k is the unit vector in the upward vertical direction, K(x,t) is the turbulent diffusivity tensor.

The condensation/evaporation rate of species i is [Wexler et al., 1994]

$$H_{i} = \frac{1}{m} \frac{dm_{i}}{dt} = \frac{2\pi D_{p} D_{i}}{m} \frac{C_{\infty,i} - C_{s,i}}{\frac{2\lambda}{\alpha_{i} D_{p}} + 1}$$
(10)

where D_i is the molecular diffusivity of species i in air, $C_{\infty,i}$ and $C_{s,i}$ are the concentrations in the bulk gas phase and at the particle surface, λ is the air mean free path, and α_i is the accommodation coefficient for species i on the atmospheric aerosol. Particle surface vapor concentrations $C_{s,i}$ are estimated by a thermodynamic routine, Simulating Composition of Atmospheric Particles at Equilibrium 2 (SCAPE2), which will be described subsequently. Equation (10) is used to compute rates of gas-aerosol transfer for sulfate, ammonia, nitric acid, hydrochloric acid, and secondary organic aerosols (SOA). Water and CO_2 (or carbonates) can be assumed to be in local, instantaneous equilibrium between the gas and aerosol phases. The condensation /evaporation rate for water is [Wexler et al., 1994],

$$H_{w} = \frac{1}{m} \frac{dm_{w}}{dt} = \sum_{i} \frac{1000 H_{i}}{M_{i} m_{0,i} (RH)} - \frac{1000}{p} \frac{\partial RH}{\partial t} \sum_{i} \frac{p_{i}}{M_{i} m_{0,i}^{2} (RH)} \frac{\partial m_{0,i} (RH)}{\partial RH}$$
(11)

where M_i is the molecular weight of species i and $m_{0,i}$ is the

molality of species i in a binary aqueous solution with water activity equal to relative humidity RH.

In a three-dimensional model, dry deposition of both gaseous and particulate species is included in the ground level boundary condition to (9) in terms of a deposition velocity $V_d = F/C(z_r)$, where F is the downward mass flux and $C(z_r)$ is the concentration at a reference height z_r (typically $z_r = 10$ m) [Russell et al., 1993]. The deposition flux is given by

$$F = [K_{zz}(z) + D] \frac{dC(z)}{dz} + V_s C(z)$$
 (12)

where K_{zz} is eddy diffusivity, D is molecular diffusivity, and V_s is the settling velocity.

3. Gas-to-Particle Conversion

3.1. Condensation/Evaporation and Nucleation

The condensation/evaporation driving force for species i is the difference between the concentration just above the particle surface $C_{s,i}$ and that in the bulk gas $C_{\infty,i}$. Most previous efforts in modeling condensation/evaporation of volatile species have assumed instantaneous gas-aerosol equilibrium. In this work condensation/evaporation processes are modeled dynamically. The thermodynamic model SCAPE2, which is described in section 3.3, is used to calculate the particle surface vapor concentrations $C_{s,i}$ in (10) for all inorganic species. Later we will compare predictions based on the fully dynamic approach with those based on the equilibrium approach, which partitions the total concentration of volatile species between the gas and bulk aerosol phases and then allocates the aerosol species to differently sized sections based on aerosol surface area [Pandis et al., 1993; Lurmann et al., 1997].

Homogeneous nucleation is assumed to occur only with H_2SO_4/H_2O . A nucleation threshold H_2SO_4 concentration C_{crit,H_2SO_4} (in μ g m⁻³) can be calculated from [Wexler et al., 1994]

$$C_{\text{cnt,H,SO}} = 0.16 \exp(0.1T - 3.5\text{RH} - 27.7)$$
 (13)

where T is in Kelvins and RH is between 0 and 1. If the ambient H_2SO_4 vapor concentration exceeds C_{cnt,H_2SO_4} , that amount exceeding the threshold is removed from the gas phase and placed in the smallest aerosol size section.

3.2. Secondary Organic Aerosol Formation

Secondary organic aerosol (SOA) results when a parent organic compound A reacts with OH, O₃, or NO₃ to yield products that have sufficiently low vapor pressures that they partition into the aerosol phase. For example,

$$A + OH \rightarrow \cdots + \nu B + \cdots$$

where the semivolatile product B formed with stoichiometric coefficient v partitions between the gas and particulate phases,

$$\mathbf{B}(g) \stackrel{\rightarrow}{\smile} \mathbf{B}(p)$$

Once the semivolatile condensable vapor B(g) is formed in the gas phase, mass transfer of B(g) to B(p) is governed by (10). Gas/particle partitioning of semivolatile organic compounds to

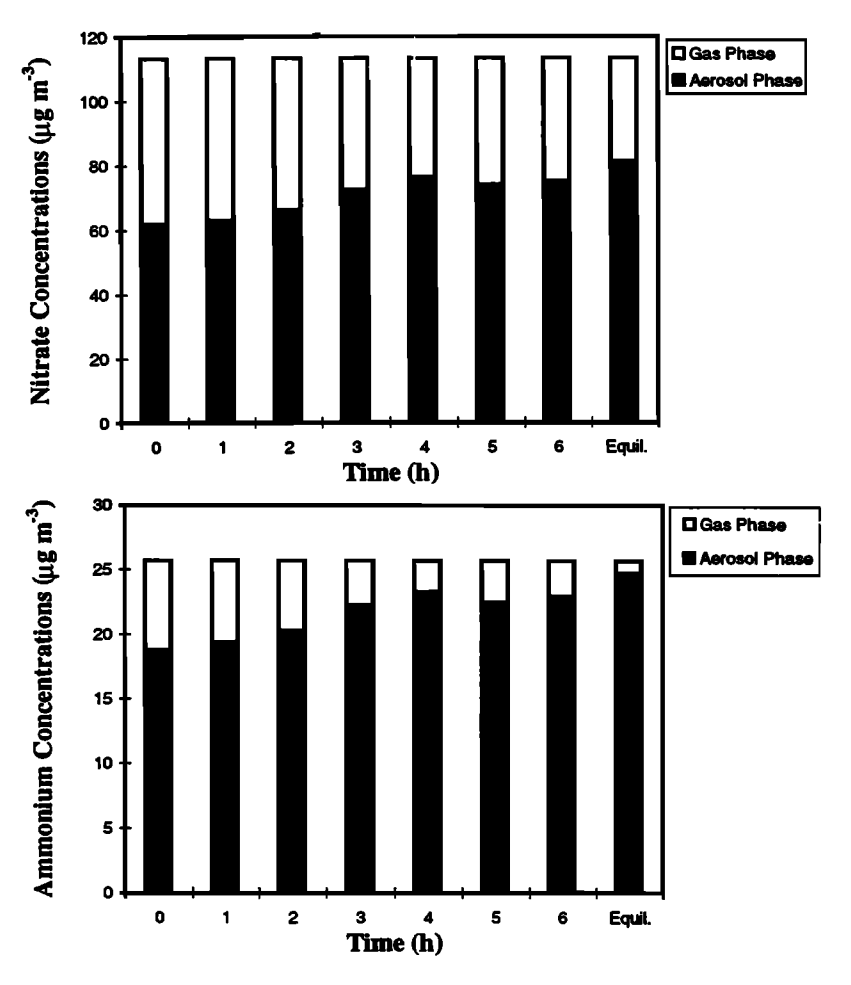


Figure 1. Comparison between partitions of the total nitrate and ammonium predicted by the dynamic model at various times and those by the hybrid method for condensation/evaporation only in a single cell.

urban particulate matter containing a significant fraction of organic matter will be dominated by absorption of the compound into the particulate organic layer [Odum et al., 1996]. On the basis of the absorption mechanism the surface vapor concentrations of semivolatile organic compounds are governed by

$$C_{s,i}^{\text{eq}} = \frac{F_i}{K_i^{\text{OM}} \text{OM}}$$
 (14)

where F_i (µg m⁻³) is the concentration of organic species i in the aerosol phase, K_i^{OM} (m³ µg⁻¹) is the absorption partitioning coefficient, and OM (µg m⁻³) is the absorbing organic mass concentration.

Aromatic species can be presumed to be the major anthropogenic sources of SOA [Odum et al., 1996; 1997]. Two condensable vapor products can be assumed to result from each of the reactions of toluene (TOLU) and higher aromatics (AROM) with OH, namely,

$$\mathsf{TOLU} + \mathsf{OH} \rightarrow ... + v_1 \mathsf{ATO1} + v_2 \mathsf{ATO2}$$

$$AROM + OH \rightarrow ... + v_1AAR1 + v_2AAR2$$

where v_1 and v_2 are stoichiometric coefficients, and ATO1, ATO2, AAR1, and AAR2 are the generalized semivolatile vapor products [Odum et al., 1996].

3.3. Aerosol Thermodynamics

SCAPE is an aerosol thermodynamic model that was first

introduced in 1993 [Kim et al. 1993a, b] and has undergone continued development since that time. It has the most complete treatment of inorganic gas-aerosol equilibrium available and provides the option of using three popular activity coefficient estimation methods (Bromley, Kusik-Meissner (KM), and Pitzer); also, with respect to RH variations one can choose to calculate either the metastable or full equilibrium state of the particles. The KM method was used in the present study, as it has been shown [Kim et al., 1993b] that this method gives more reasonable results than the other two in concentrated solutions when compared against available experimental data. The ZSR method [Robinson and Stokes, 1965] is used to estimate water activity because of its computational efficiency and comparable accuracy with other more complex methods. Temperature dependence of deliquescence points is also considered. The original version of SCAPE includes sodium, sulfate, ammonium, nitrate, and chloride. Subsequent work has added potassium, calcium, magnesium, and carbonates [Kim et al., 1995; Meng et al., 1995a].

In the original version of SCAPE the equilibrium relations, together with mass balance and electroneutrality conditions, are reduced to a single equation in the H^+ concentration. After gaseous and aqueous species concentrations are obtained, solid concentrations in the aerosol phase are calculated. The original version of SCAPE cannot be used directly to calculate the particle surface vapor concentrations $C_{s,i}$. We have modified the original version and have developed an option to handle aerosol-phase-only thermodynamics. The new version is termed SCAPE2. In

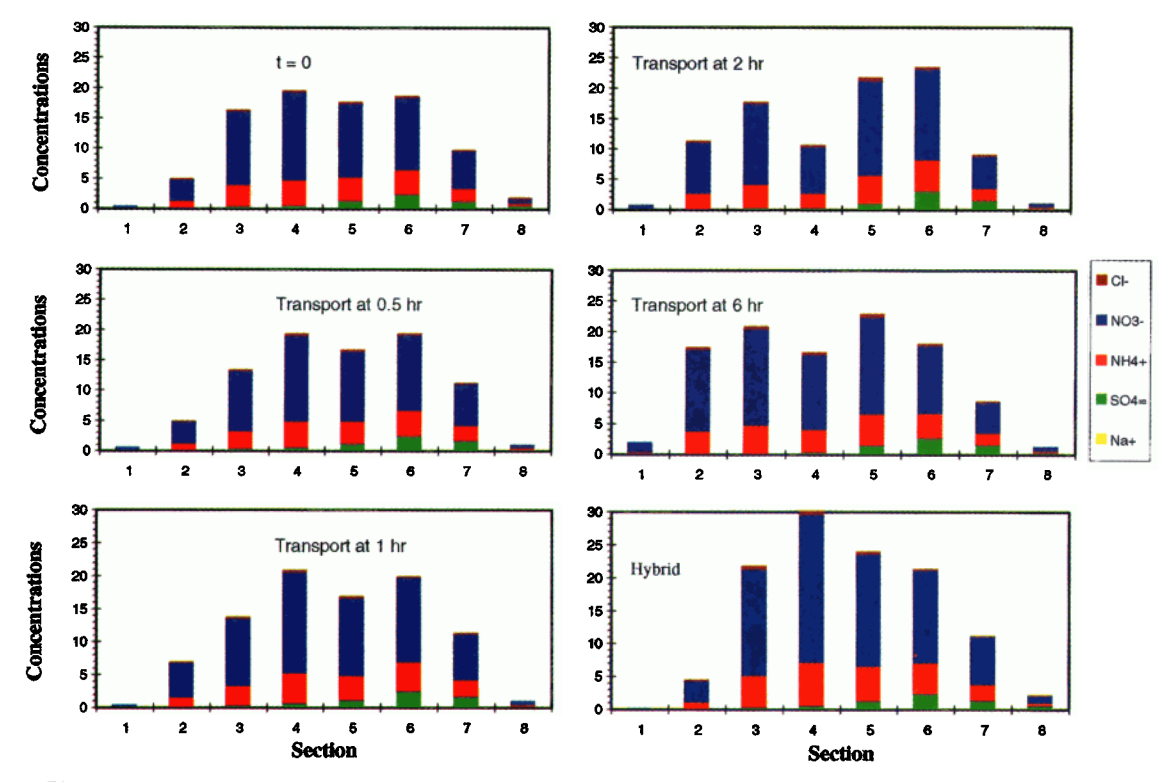


Plate 1. Size-resolved and composition-resolved aerosol distributions predicted by the dynamic model at various times and that predicted by the "hybrid" method for condensation/evaporation only in a single cell.

determining the H⁺ concentration the original SCAPE uses the combined bisection-Newton method; in SCAPE2, only the bisectional method is applied to the logarithmic scale of the concentration domain.

Crustal compounds affect the general equilibria of volatile species. When the aerosol contains water, crustal species alter the ion balance and interactions. For pure solid particles the following heterogeneous chemical reactions are relevant,

$$\begin{array}{ccccc} \text{HNO}_3 + \text{NH}_4\text{Cl} & \xrightarrow{\leftarrow} & \text{NH}_4\text{NO}_3 + \text{HCl} \\ \text{HNO}_3 + \text{NaCl} & \xrightarrow{\leftarrow} & \text{NaNO}_3 + \text{HCl} \\ \text{HNO}_3 + \text{KCl} & \xrightarrow{\leftarrow} & \text{KNO}_3 + \text{HCl} \\ \text{HNO}_3 + \frac{1}{2}\text{CaCl}_2 & \xrightarrow{\leftarrow} & \frac{1}{2}\text{Ca(NO}_3)_2 + \text{HCl} \\ \text{HNO}_3 + \frac{1}{2}\text{MgCl}_2 & \xrightarrow{\leftarrow} & \frac{1}{2}\text{Mg(NO}_3)_2 + \text{HCl} \end{array}$$

where the equilibrium constants for the above five reactions, K_1 , K_2 , K_3 , K_4 , and K_5 , are 1.8908, 4.0075, 12.694, 1461.7, and 2489.5, at 298 K, respectively. If surplus HNO₃ vapor is present, it reacts preferentially with MgCl₂ if available, then CaCl₂, KCl, NaCl, and NH₄Cl, on the basis of the values of their equilibrium constants. For instance, if reaction of HNO₃ and NaCl is to proceed, nitric acid must have consumed the available KCl, CaCl₂, and MgCl₂ already. The reverse is true if excess HCl is available for reaction with the nitrate salts, though this situation is less likely in the atmosphere. Similar considerations apply to reactions of the carbonate salts with HNO₃ and HCl.

4. Numerical Solution

Operator splitting [McRae et al., 1982] is used to solve the different physical and chemical processes according to the following order, $T_xT_yT_{z,c}T_aT_yT_x$, where T_x , T_y , $T_{z,c}$, and T_a represent the operators of transport in x direction, transport in y direction, transport in y direction and gas-phase chemistry, and aerosol dynamics, respectively. Spatial advection and diffusion terms in the above equation are solved by the same methods as in the host gas-phase atmospheric chemical transport model.

The aerosol operator is activated after the gas-phase chemistry operator is finished; it calculates mass transport between the gas and aerosol phases while total mass concentrations are conserved. The numerical time step for the mass transport varies according to the characteristic mass transport timescale and Courant number at the beginning of each time step and is determined by the smallest of these for all the aerosol size sections. Whether or not the particle surface vapor concentrations for a particular size section are updated at a given time step by "calling" the aerosol thermodynamic model (SCAPE2) is determined by the ratio of the time passed since the last update over the previous characteristic timescale for that section. The aerosol operator becomes inactive after the mass transport has proceeded for a time step of the gas-phase chemistry operator.

Representation of the size-resolved and composition-resolved aerosol distribution function is based on a sectional approach. An internal mixture is assumed for the particles; that is, within each size section the chemical composition of the particles is unique, and furthermore, the mass concentration distribution of a given species is assumed to be constant in a given size section. The particle size domain is divided into 8 size sections, with two coarse sections between 2.5 μ m and the largest size boundary $D_{p, \max}$, and six sections between the lowest size boundary $D_{p, \min}$

Table 5. Boundary Conditions for Chemical Species Considered in the Model

Species Name	Mixing Ratio, ppb	Species Name	Concentration, µg m ⁻³
NO	1	PM _{2.5} NO ₃	1.7
NO ₂	1	PM _{2.5-10} NO ₃	0.56
O_3	60	$PM_{2.5} NH_4^+$	0.90
HNO ₃	0.01	PM _{2.5-10} NH ₄ ⁺	0.27
со	200	$PM_{2.5} SO_4^{2-}$	1.2
нсно	3	PM _{2.5-10} SO ₄ ²⁻	0.30
Acetaldehyde	5	PM _{2.5} Cl	0.26
Methyl ethyl ketone	4	PM _{2.5-10} Cl	0.26
C ₄ ⁺ alkanes	9.5	PM _{2.5} Na ⁺	0.22
Ethene	1.7	PM _{2.5-10} Na	0.18
C ₃ ⁺ alkenes	1.8	$PM_{2.5} H_2O$	0.12
Toluene	1.5	$PM_{2.5-10}H_{2}O$	0.03
Higher aromatics	1.6	PM _{2.5} EC	0.14
NH ₃	0.1	PM _{2.5-10} EC	0.02
SO ₂	1	PM _{2.5} Primary OM	3.04
CH ₄	2200	PM _{2.5-10} Primary OM	1.01
HCl	0.01	PM ₂₅ Other	3.67
HCl		PM _{2.5-10} Other	1.12

Values are based on *Harley et al.* [1993] and *Lurmann et al.* [1997]. Chemical species not listed have boundary conditions equal to zero.

and $2.5~\mu m$. $D_{p,max}$ is chosen to be $10~\mu m$ in this study. The equidistant spacing in the logarithmic scale of the size domain dictates that the lowest size boundary is $0.039~\mu m$. (PM $_{2.5}$ and PM $_{10}$ denote particles with diameter smaller than $2.5~\mu m$ and $10~\mu m$.) If particles grow beyond $D_{p,max}$, their sizes are reduced and the number concentration is increased to maintain mass conservation; on the other hand, if the particles shrink below $D_{p,min}$, their sizes are increased and the number concentration is reduced. The above treatment of the upper and lower boundary conditions has a negligible influence on model predictions because, when the particle size spectrum is sufficiently broad, the mass fractions of particles outside the boundaries are small and small particles (sulfate dominant) are more likely to experience condensation than evaporation at the lower particle size boundary.

The condensation/evaporation term is solved by Bott's method [Dhaniyala and Wexler, 1996]. Numerical solution of the condensation/evaporation portion of (9),

$$\frac{\partial p_i(\mu, t)}{\partial t} = H_i(\mu, t) p(\mu, t) - \frac{1}{3} \frac{\partial H p_i(\mu, t)}{\partial \mu}$$
 (15)

is given by

$$[p_{i}]_{j}^{n+1} = [p_{i}]_{j}^{n} + \frac{[H_{i}]_{j}}{[H]_{j}} [p_{i}]_{j}^{n} [\exp(H\Delta t) - 1]$$
$$-\frac{\Delta t}{\Delta u} \Big(F_{j+1/2}^{n} - F_{j-1/2}^{n} \Big)$$
(16)

where n denotes the discretized time t, j is the discretized size domain (μ) , Δt and $\Delta \mu$ are the time step and section width, and $F_{j+1/2}^n$ and $F_{j-1/2}^n$ are the p_i fluxes through the right and left boundaries of section j. Numerical values of the fluxes $F_{j+1/2}^n$ and $F_{j-1/2}^n$ are obtained by integration of the net outflow mass as a result of particle growth or shrinkage, on the basis of polynomial approximation of the distribution function. These fluxes are then normalized by the actual available mass so that the numerical scheme is positive-definite. After comparing it with other numerical methods for solving the condensation/evaporation process, Dhaniyala and Wexler [1996] found that Bott's method is accurate and numerically very efficient

Before (15) or (16) can be solved one needs to evaluate the growth rate H_i according to (10), which requires estimation of surface vapor concentrations $C_{s,i}$. For sulfuric acid we assume, because of its extremely low vapor pressure, the surface vapor concentration to be zero for all particles. Vapor concentrations for the volatile inorganic compounds, namely, NH_3 , HNO_3 , and HCl, are estimated by the thermodynamic model SCAPE2, as described earlier. At the beginning of the aerosol time step, SCAPE2 is called to calculate the growth rates for all the inorganic aerosol components except water and carbonates. Growth rates for aerosol water and carbonates are calculated as follows,

$$H_{\text{wat}} = H_{\text{w.adi}} + H_{\text{w}}, \qquad H_{\text{car}} = H_{\text{c.adi}} + fH_{\text{w}}$$
 (17)

where H_w is defined in (11), f is the mass ratio of carbonate to water, and the adjusted growth rates $H_{w,\mathrm{adj}}$ and $H_{c,\mathrm{adj}}$ are calculated by

$$H_{\text{w,adj}} = \frac{1}{m} \frac{\Delta m_{\text{w}}}{\Delta t}, \quad H_{c,\text{adj}} = \frac{1}{m} \frac{\Delta m_{c}}{\Delta t}$$
 (18)

where Δm_w and Δm_c are the differences between the equilibrium-update water content and carbonates calculated at the beginning of the current aerosol time step and those from the previous time step. The mass change of carbonates is adjusted on the basis of the change of aerosol water content.

Both sequential and parallel versions of the model have been implemented on IBM RISC 6000 computers. About 72 CPU hours are required for a typical 1-day simulation of the South Coast Air Basin of California on a single IBM 390 computer, while the parallelized version requires about 14 hours running on 5 IBM 390 nodes. More than 95% of the CPU time associated with the aerosol model is consumed in calculating aerosol thermodynamics.

5. Dynamic Versus Hybrid Approaches

This work uses a dynamic approach to calculate detailed mass transfer of volatile species between the gas phase and size-resolved particles. An equilibrium-based "hybrid" method has been used in some previous aerosol studies [Pandis et al., 1993; Lurmann et al., 1997]. The hybrid method first calculates at any

Table 6. Total Emissions for Each Chemical Species for August 28, 1987

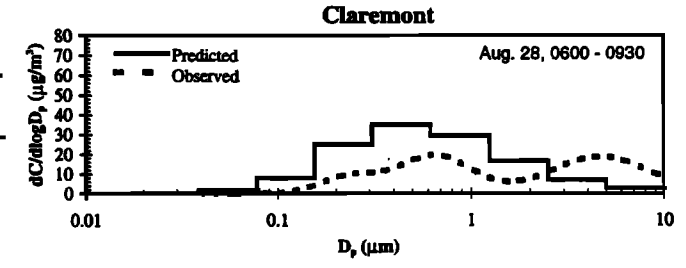
	Total, kg
ALD2	20,505
ALKA	939,353
ALKE	148,475
AROM	174,214
Cl<2.5 μm	11,780.88
Cl 2.5-10 µm	28,614
CO	5,488,410
EC<2.5 μm	29,503
EC 2.5-10 μm	8,224
ETHE	136,327
ЕТОН	99,362
нсно	32,436
ISOP	89,493
MEK	50,345
MEOH Na<2.5 μm	4,724 7,854
•	ŕ
Na 2.5-10 μm	19,108
NH ₃	166,109
NO NO ₂	699,129 56,362
Ol < 2.5 μm	195,302
Ol 2.5-10 μm	559,241
OO<2.5 μm	93,936
OO 2.5-10 μm	143,582
Sf <2.5 μm	13,911
Sf 2.5-10 μm	6,893
SO ₂	135,884
SO ₃	3,533
TOLU	214,296

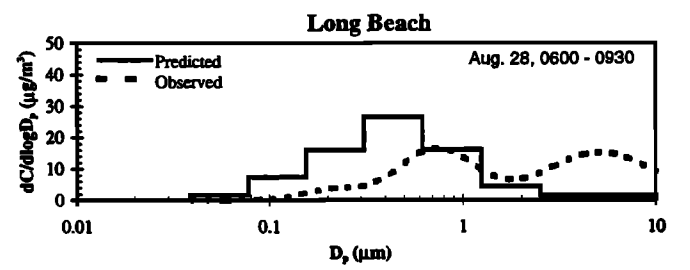
The sources are *Harley et al.* [1993] and *Wagner and Allen* [1990] where the abbreviations are defined as follows:

ALD2, lumped aldehyde; ALKA, >C3 alkanes; ALKE, >C2 alkenes; AROM, aromatics; Cl, chloride; CO, carbon monoxide; EC, elemental carbon; ETHE, ethene; ETOH, ethanol; HCHO, formaldehyde; ISOP, isoprene; MEK, methyl ethyl ketone; MEOH, methanol; Na, sodium; NH₃, ammonia; NO, nitric oxide; NO₂, nitrogen dioxide; Ol, crustal; OO, other organic species; Sf, sulfate; SO₂, sulfur dioxide; SO₃, sulfur trioxide; and TOLU, toluene.

instant of time the equilibrium for volatile compounds between the gas and bulk aerosol phases and, then distributes the aerosol mass increment over the size spectrum based on a particle surface area weighting.

The dynamic approach can simulate mass transfer between the gas phase and individual aerosol particles whereas the hybrid approach computes only overall gas-aerosol equilibrium. For example. Plate 1 shows a comparison between predictions by the dynamic and hybrid methods. Initial gas-phase concentrations are 10 ppb NH₂ (6.95 μ g m⁻³), 20 ppb HNO₂ (51.52 μ g m⁻³), and 2 ppb HCl (2.98 µg m⁻³). Initial size-resolved and chemically resolved aerosol concentrations are taken to be those at t = 0 in Plate 1. Temperature is assumed to be 298 K, and relative humidity is 80%. Only condensation/evaporation is considered in this example; all other physical and chemical aspects, such as deposition and emissions, are ignored. The condensation/ evaporation rate is controlled by the difference between the concentration in the bulk gas phase and that at the particle surface, the single-particle surface area, and the total number of particles in the size section. Initially, particles in the third and





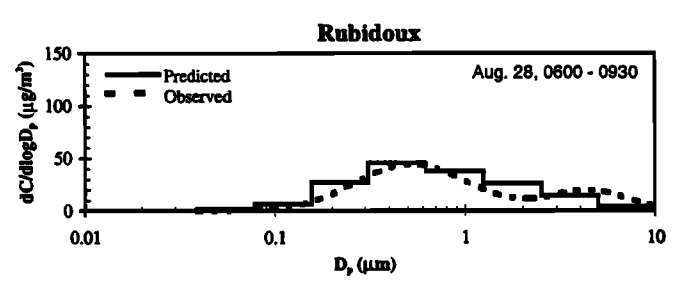
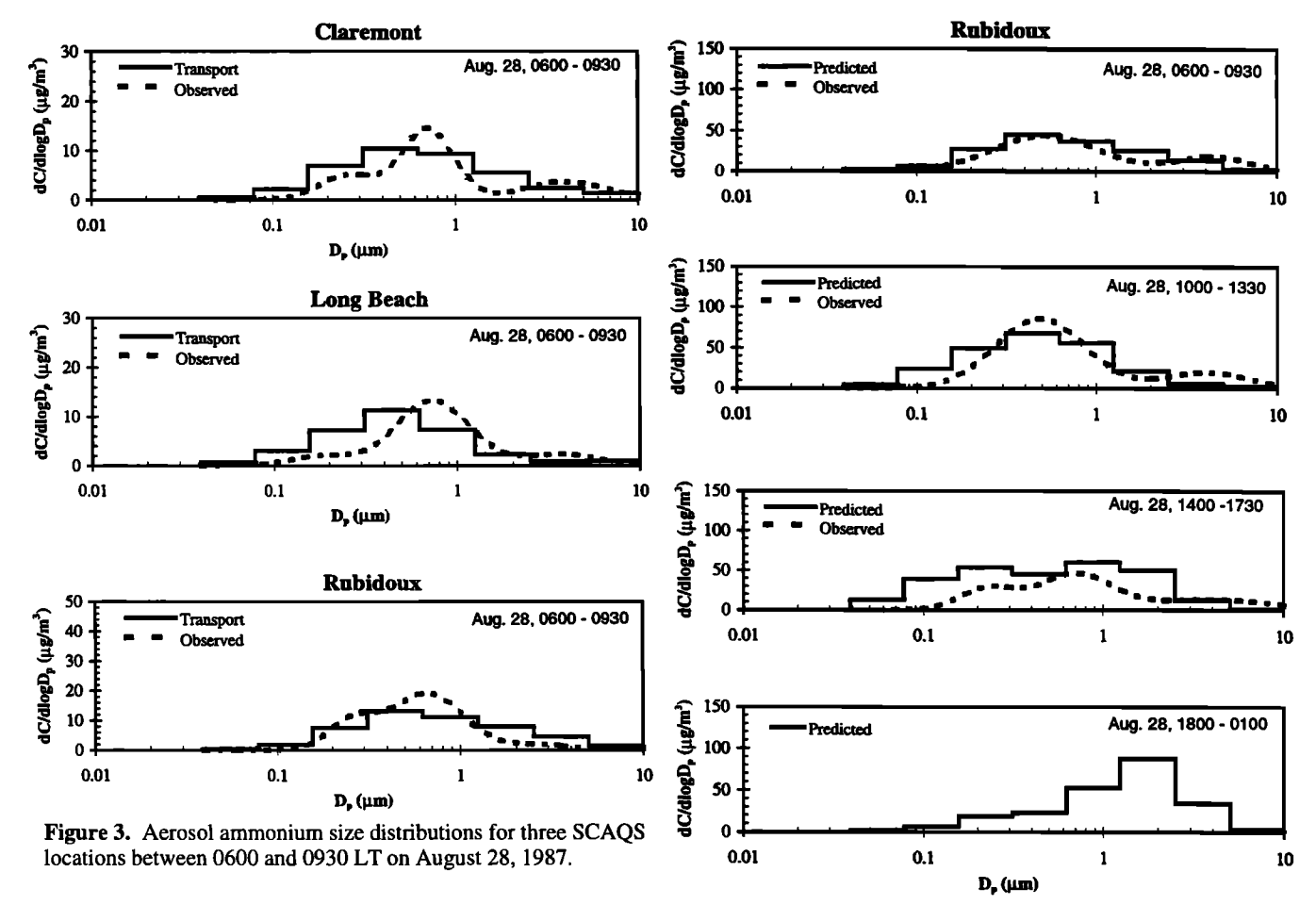


Figure 2. Aerosol nitrate size distributions for three South Coast Air Basin locations between 0600 and 0930 LT on August 28, 1987. Air samples were taken with Berner Impactors at the intensive Southern California Air Quality Study (SCAQS) sampling sites and analyzed for various inorganic ions. The impactor stage masses were transformed by a data reduction algorithm into mass size distributions and then fitted with lognormal functions. The measured aerosol size distributions presented are reconstructed from the fitted lognormal parameters.

fifth size sections are more acidic than those in other size sections, and particles in these two size sections experience some evaporation of NHANO, even as NHANO, is condensing on particles of other sizes. At 2 hours the concentrations in the fourth section have decreased because the original particles in this section have grown to larger particle sizes while those in the third section have not grown fast enough to reach the fourth section. Changes in the aerosol size distribution after about 6 hours are negligible. That distribution, however, is quite different from that predicted by the hybrid method on the basis of the equilibrium between bulk gas and aerosol phases and the initial size distribution. The reason for this difference is that the hybrid method does not account for the chemistry of individual particles. The predicted partition of total nitrate and ammonium between the gas and bulk aerosol phases by the two approaches is shown in Figure 1. In this case the hybrid method just gives the equilibrium partitioning. After 6 hours, even though the size distributions are different, the overall gas-aerosol partitioning predicted by the dynamic model is close to the equilibrium value. In three-dimensional aerosol modeling this may not be the case since total nitrate and ammonium concentrations in a grid cell at a particular time will vary depending on the approach used. For instance, as a result of mass-transport limitation, the dynamic



model may predict higher gaseous HNO₃ concentrations at a particular location and time than equilibrium would indicate. Because HNO₃ has a considerably larger dry deposition velocity than aerosol nitrate, the total nitrate concentration could, as a result, be noticeably reduced from that predicted on the basis of instantaneous local equilibrium as a result of the larger loss of HNO₃.

6. Simulation of an Episode in the South Coast Air Basin of California

We present the simulation of a 3-day episode in the South Coast Air Basin of California (SoCAB) from August 27-29, during the summer 1987 SCAQS. High ozone (>240 ppb) and PM_{10} (> 100 μg m⁻³) levels were measured during this episode. The highest measured ozone concentration for this period was observed at Glendora on August 28, with a peak 1-hour average mixing ratio of 290 ppb. *Jacobson* [1997] has also simulated this period.

Wind flow during the 3-day period was generally characterized by sea breeze during the day and a weak land-mountain breeze at night. Weak onshore pressure gradient and warming temperatures aloft increased the potential for photochemical ozone formation on August 27. Low clouds penetrated into the coastal valleys on August 28, with pressure gradients still remaining weak onshore. The weak upper trough along the coast on August 29 lifted the inversion base and created a slight reversal of the pressure gradient, resulting in inland penetration of the morning low clouds and fog to the coastal valleys. Over the 3-day period, there

Figure 4. Aerosol nitrate size distributions at Rubidoux (Riverside), California, for various sampling periods on August 28, 1987.

existed well-defined inversion layers atop neutral and unstable layers near the surface. The inversion base height field is derived from potential temperature analysis of air soundings [Harley et al., 1993]. Nocturnal ground-based inversions for August 27-29 were observed only at inland locations. The nocturnal boundary layer was generally slightly stable or near neutral. At all times and locations the inversion base heights are within the maximum vertical extent of the model domain.

6.1. Gas-Phase CIT Model

The "host" gas-phase chemical-transport model is the three-dimensional CIT model [McRae et al., 1982; McRae and Seinfeld, 1983; Harley et al., 1993]. Three-dimensional meteorological data are constructed through data interpolation with a diagnostic wind model [Goodin et al., 1979, 1980]. The horizontal grid domain is 80×30 , with a resolution of 5 km. Five vertical layers extend to a height of 1100 m above ground level. Gas-phase chemistry is based on the chemical mechanism of Lurmann et al. [1987] with extensions by Harley et al. [1993]. The species in the chemical mechanism are listed in Table 5. The original mechanism includes 35 chemical species, of which eight are lumped species representing organic compounds of similar reactivity. Hydrochloric acid (HCl) has been added to the original gas-phase chemical mechanism. A constant CH₄ mixing ratio of 2.2 ppm is assumed. Isoprene is used as a surrogate for all

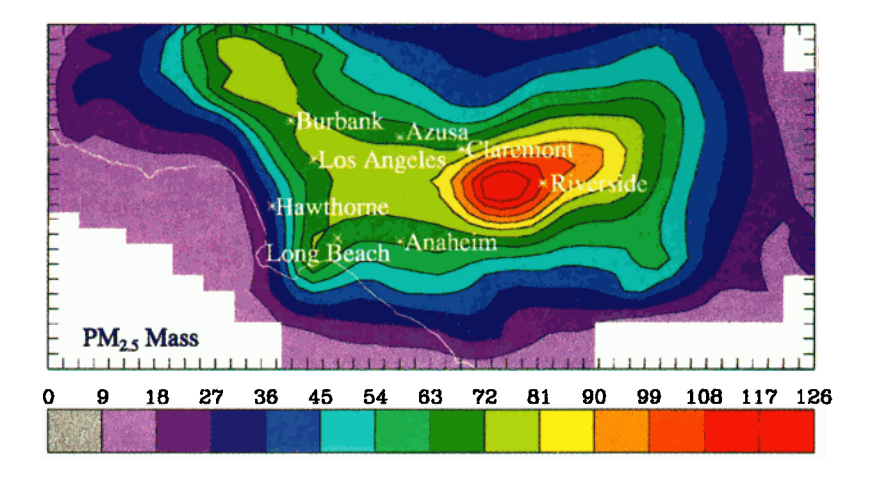


Plate 2. Predicted 24-hour mean $PM_{2.5}$ mass concentrations ($\mu g \ m^{-3}$) on August 28, 1987, in South Coast Air Basin. The distance between tick marks on the axes is 5 km.

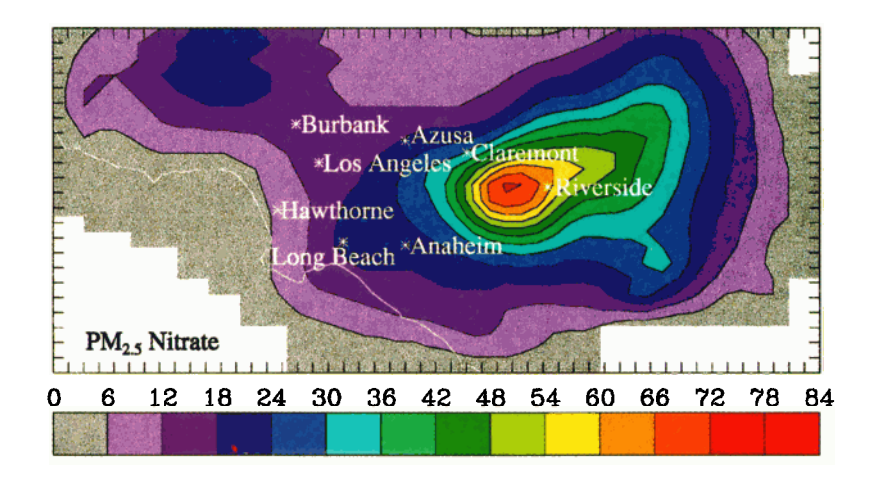


Plate 3. Predicted 24-hour mean $PM_{2.5}$ nitrate concentrations ($\mu g \ m^{-3}$) on August 28, 1987, in South Coast Air Basin. The distance between tick marks on the axes is 5 km.

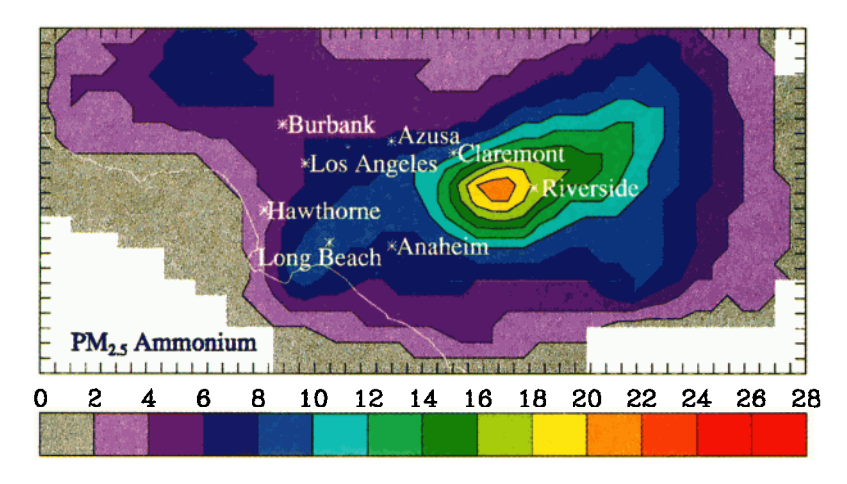


Plate 4. Predicted 24-hour mean $PM_{2.5}$ ammonium concentrations (µg m⁻³) on August 28, 1987, in South Coast Air Basin. The distance between tick marks on the axes is 5 km.

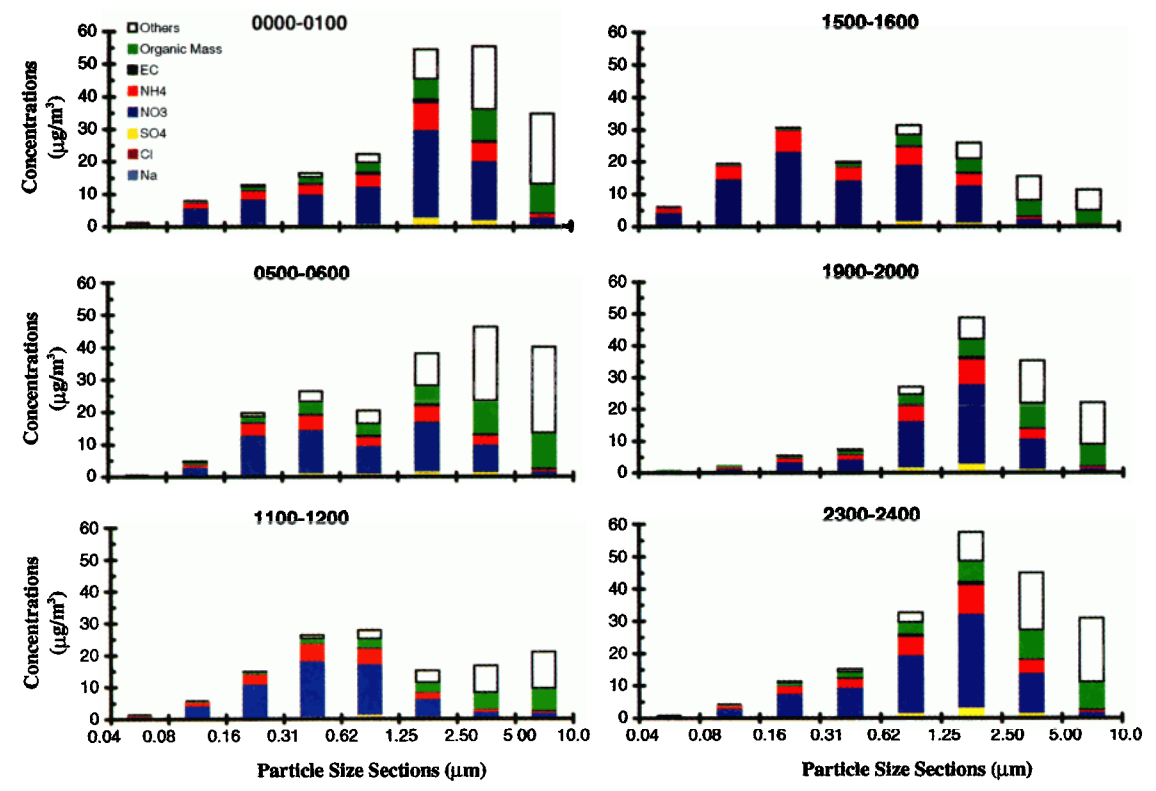


Plate 5. Size-resolved and composition-resolved aerosol distributions at Riverside, California, at various times on August 28, 1987. Water concentration is not shown.

biogenic hydrocarbon emissions. Since isoprene does not yield secondary organic aerosol [Pandis et al., 1992a], the current simulation includes SOA only from anthropogenic aromatic compounds.

6.2. Emissions

Emission data for gaseous compounds are described by Harley et al. [1993]. In brief, day-specific pollutant emission inventories for the August 1987 episode were received from the California Air Resources Board (CARB) [Wagner and Allen, 1990]. The mobile source emissions estimates [Yotter and Wade, 1989] were adjusted to account for daily temperature variations. On-road vehicle hot exhaust emissions of CO and hydrocarbons were increased to 3 times the base values to reflect realistic on-road vehicle emission rates [Harley et al., 1993]. Stationary source emissions, which include day-specific power plant, aircraft, and refinery sources, were prepared by the South Coast Air Quality Management District (SCAQMD). The NH₂ emissions inventory used was developed by Cass and Gharib [1984]. SO₂ emissions and chemically resolved and size-resolved primary particle emissions used are those presented by Lurmann et al. [1997]. Particle emissions account for six chemical species: sulfate, elemental carbon (EC), organic material (OM), sodium, chloride, and "other" species. Ammonium and nitrate from primary emissions are small and can be neglected. A value of 75 t d⁻¹ is assumed for NaCl emissions following Lurmann et al. [1997]. The total amount of NaCl emissions is uniformly distributed over the computational domain, and the daily emissions are divided by 24 hours to obtain the hourly emissions within each grid cell. There are four size ranges for aerosol mass in the CARB PM emission profiles; they are, <1, 1-2.5, 2.5-10, and >10 μ m. Because the emission profiles are coarser than the size resolution

for a typical aerosol simulation, for each species and source category a continuous size distribution was estimated to distribute the original emissions data to a finer size resolution for a particular simulation. The estimated continuous size distributions were based on a modified version of Twomey's algorithm for inversion of the cascade impactor data to generate the aerosol size distribution [Winklmayr et al., 1990]. The original CARB PM profiles have been distributed over the eight size sections for the current implementation. Table 6 presents total emissions for each species for August 28, 1987.

6.3. Initial and Boundary Conditions

Boundary and initial conditions for the episode are specified using routine surface level air quality measurements and aircraft-based measurements acquired during SCAQS [Harley et al., 1993]. PM₁₀ data are based on the monthly average [Lurmann et al., 1997]. The initial size-resolved and composition-resolved aerosol concentrations are provided by Lurmann et al. [1997], which were estimated on the basis of the annual averages in SoCAB [Solomon et al., 1988] and were distributed to the eight size sections used in the simulations. Since estimated initial concentrations are close to the actual PM_{2.5} measurements at midnight on August 27, 1987, it was not necessary to develop initial conditions based on the measured PM_{2.5} concentrations at midnight on August 27, 1987. Boundary concentrations above the mixing height are given in Table 5.

6.4. Simulation Results

Predicted 24-hour average PM_{2.5} mass concentrations on August 28 are shown in Plate 2. A band of high concentrations extending from northwest to southeast in the region is predicted,

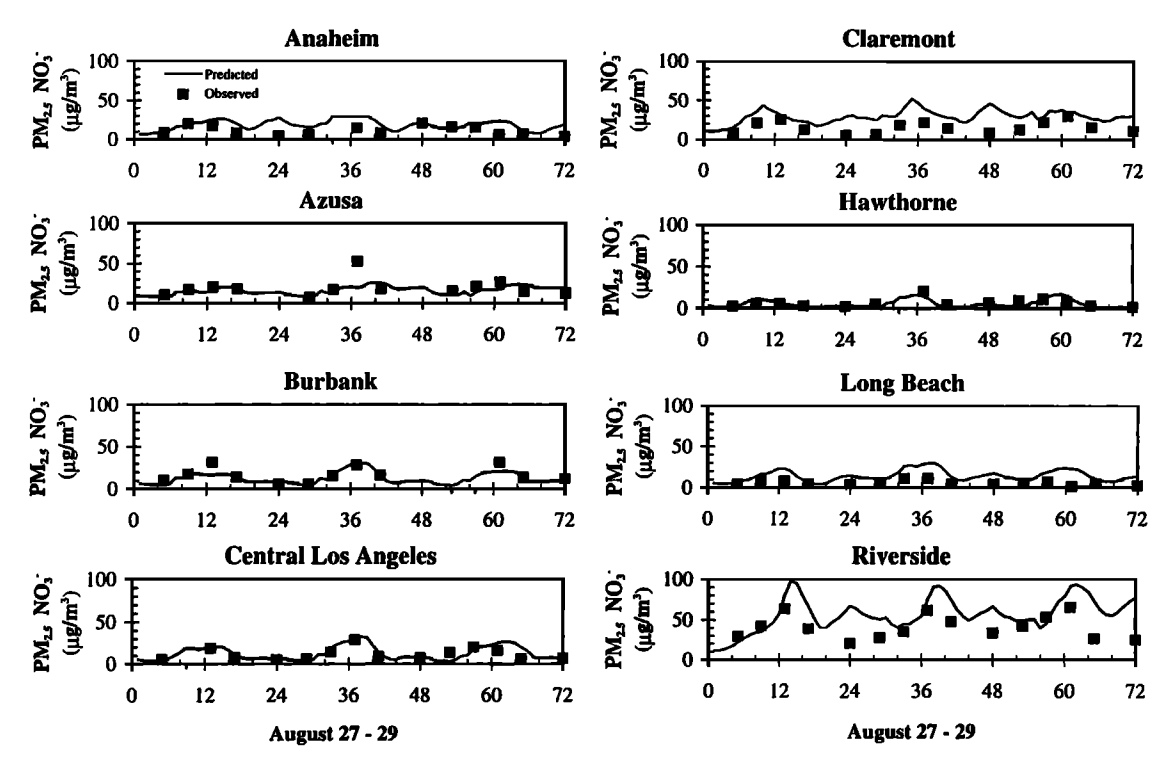


Figure 5. Time-series of predicted and observed PM_{2.5} nitrate concentrations at various locations during August 27-29, 1987.

with a maximum reached near Riverside. Although not shown, the maximum predicted PM_{10} mass concentration is about 45% higher than the $PM_{2.5}$ mass. Predicted 24-hour average $PM_{2.5}$ nitrate and ammonium mass concentrations on the same day are shown in Plates 3 and 4. Both exhibit spatial patterns similar to those of total PM mass concentrations.

Predicted size distributions of aerosol nitrate and ammonium are compared with available measurements [John et al., 1989] on August 28 between 0600 and 0930 LT at three locations in Figures 2 and 3, respectively. The simulations exhibit the submicron mode of the size distribution but do not predict the presence of the observed supermicron nitrate mode. In examining the sodium and chloride size distributions for the same period (not shown) we found that an observed single coarse mode was considerably underestimated. An underestimate of NaCl in the coarse mode will lead to an underestimate of nitrate in two ways. First, less NaCl will be available for reaction with gaseous HNO, to produce coarse mode aerosol nitrate; second, an underestimate of NaCl also implies that less coarse mode surface area is available for condensation of NH₄NO₃. A more accurate estimate of size-resolved NaCl emissions would likely improve predictions of the coarse-mode aerosol distribution.

Figure 4 shows predicted nitrate size distributions at Rubidoux, the location of the maximum in both nitrate and ammonium, for various sampling periods on August 28. In the early morning, two modes were observed for both species, nitrate being more pronounced. The submicron mode is centered at ~0.5 μ m, and the coarse mode is at ~4.0 μ m. Between late morning and early afternoon the aerosol size distribution narrows as a result of condensation, and the submicron mode diameter shifts toward larger sizes. The coarse mode remains little changed. During late afternoon, two submicron modes become evident, with the larger submicron mode growing to a diameter of ~0.7 μ m. During the evening (observations not available) the model predicts

continuous growth of the aerosol particles to a mode diameter of $\sim 2~\mu m$. Throughout the aging of the aerosol size distribution, predicted and measured NH_4NO_3 size distributions are in good agreement. The overall mass of sulfate was underestimated. This is almost certainly a result of the neglect of fog processing, which occurred in the coastal regions in the late night and early morning of August 28-29 [Pandis et al., 1992b].

Plate 5 shows predicted 1-hour average aerosol concentrations as a function of size at various times during August 28 for Riverside. Sulfate, nitrate, ammonium, and EC primarily reside in fine (PM₂₅) particles, while crustal (other) species are in coarse (PM₁₀) particles. Organic matter that is dominated by primary emissions is present in all size sections. Sodium and chloride are predicted to be minor constituents of the aerosol phase. Inland locations, such as Claremont and Riverside, are predicted to have higher NH, NO, concentrations than coastal and central basin locations. During daytime, condensation of NH, NO, causes smaller particles to grow faster than larger particles. For instance, at Riverside the peak of the accumulation mode grows from the fourth section (0.31-0.62 µm) at 0600 LT to the fifth section (0.62-1.25 µm) at 1200 LT. However, dry deposition of particles competes with particle growth. This can be seen from the decrease of the total mass concentrations from 0600 to 1200 LT, particularly for the larger particles, although condensation of NH₄NO₃ shifts the peak to larger particle size. Since evaporation of volatile compounds would shift the submicron mode peak to a smaller particle size and would have no effect on the overall concentration of crustal species (other) in the bulk aerosol phase, the decrease in aerosol concentrations at noontime is a direct result of dry deposition. Note that as expected, dry deposition has a larger effect on smaller and larger particles than on those of intermediate size (~1 µm). At 1600 LT, a bimodal size distribution is formed for the submicron particles. At 2000 LT, continued growth causes the NH₄NO₃ concentration

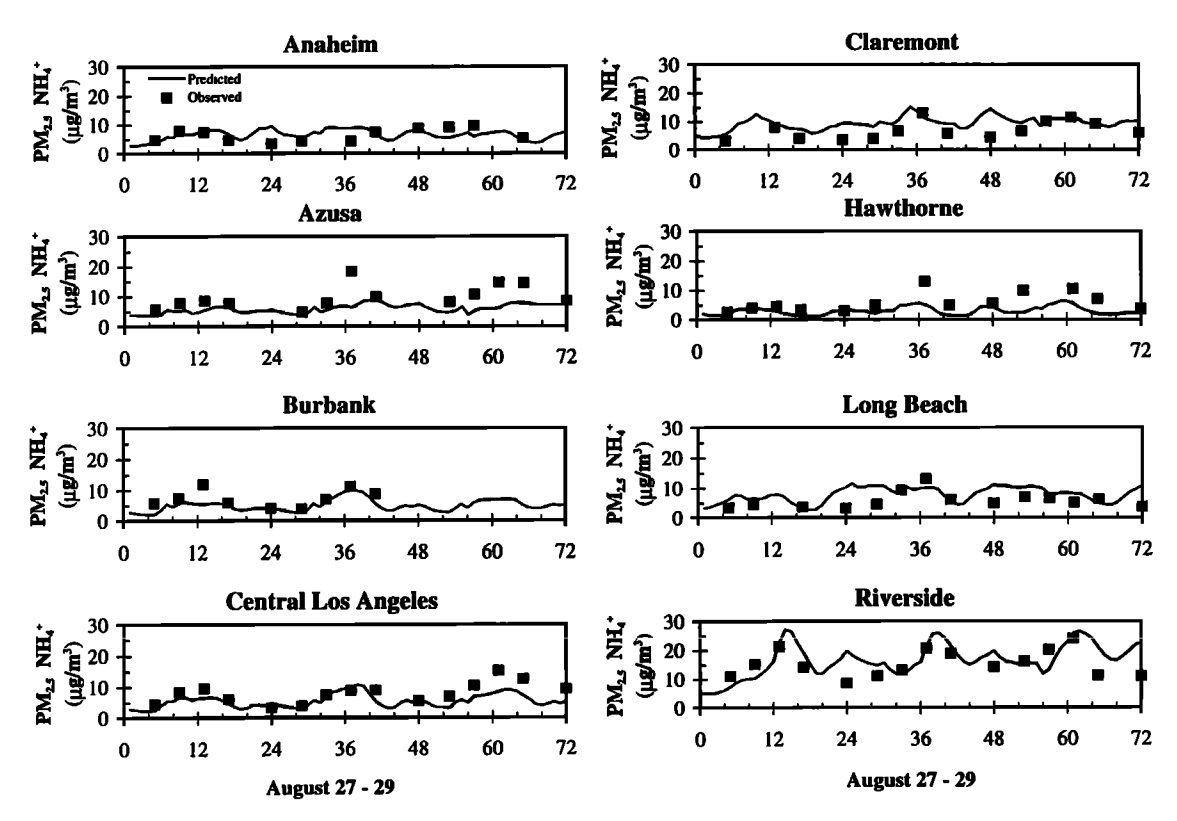


Figure 6. Time-series of predicted and observed PM_{2.5} ammonium concentrations at various locations during August 27-29, 1987.

to peak at a supermicron particle size. Note that a large fraction of the small particles is also removed by dry deposition. By midnight the aerosol size distribution attains a shape similar to that at the previous midnight.

7. Model Performance

An uncertainty analysis involves three aspects: (1) a sensitivity analysis of the model, that is, a computation of how the model predictions vary in response to uncertainties in model input variables and parameters; (2) an uncertainty analysis of the observations against which the model predictions are to be compared; and (3) a statistical evaluation of the degree of overlap between the uncertainty band generated by the sensitivity analysis and that inherent in the observations themselves. In the present case a full sensitivity analysis of the aerosol model is feasible; what is required are intelligent estimates of uncertainties in inputs, such as the emission inventory, boundary conditions, etc., and extensive computing with the model. (This computing step is nontrivial with a model of the size considered here.) Such an analysis is beyond the scope of the present paper. Aspect 2 is where the problem arises; there are virtually no estimates of the levels of uncertainty inherent in the key observation variables, the size-resolved aerosol chemical compositions. This is simply a result of the lack of multiple measurement methods that would afford one such an estimate of uncertainty. Given the absence of uncertainties stated by those who actually performed the measurements, one is hesitant to guess at levels of uncertainty. At this point the published data must simply be taken as the observed variables against which model performance is judged in the absence of error bounds. As a result, one must settle for a statistical analysis of observations and predictions, which is what is presented here.

Predicted gaseous and PM_{2.5} and PM₁₀ species concentrations have been compared against available measurements. Both PM_{2.5} and PM₁₀ samples were collected on Teflon or prefired quartz fiber filters that were then analyzed to determine aerosol mass, trace element, ionic species, and organic and elemental carbon [Countess, 1989]. PM_{2.5} NO₃ samples were collected by both Teflon filter and denuder difference method. PM_{2.5} NH₄ concentrations were measured by both Teflon filter and backup quartz filter impregnated with oxalic acid after NH₃ removal by denuder. However, some of the PM_{2.5} ammonium samples by the denuder method at Riverside were contaminated because of the high ammonia concentrations having overloaded the NH₃ denuder [Hering et al., 1997]. Five samples were taken each day with sampling periods of 4 hours during the daytime and 5-7 hours during the nighttime.

Predicted PM $_{2.5}$ nitrate and ammonium concentrations are compared with measurements in Figures 5 and 6, respectively. Note that model predictions are 1-hour averages, while measurements are averages over 4-7 hours. Statistical analysis of performance by the model based on 24-hours means is presented in Tables 7 and 8. Error analysis is carried out only for species with observed concentrations exceeding 1 μ g m $^{-3}$.

7.1. Nitrate

The predicted time series $PM_{2.5}$ nitrate (Figure 5) agrees well with observations. Overpredictions occur more frequently than underpredictions. Predicted 24-hour means of $PM_{2.5}$ nitrate averaged over the eight SCAQS observation stations are 18.3, 23.9, and 22.9 μ g m⁻³, which are higher than the 14.6, 17.2, and 16.4 μ g m⁻³ measured on August 27, 28, and 29, respectively. Predicted 24-hour means averaged over the eight SCAQS observation stations of PM_{10} nitrate are 20.7, 26.5, and 25.4 μ g

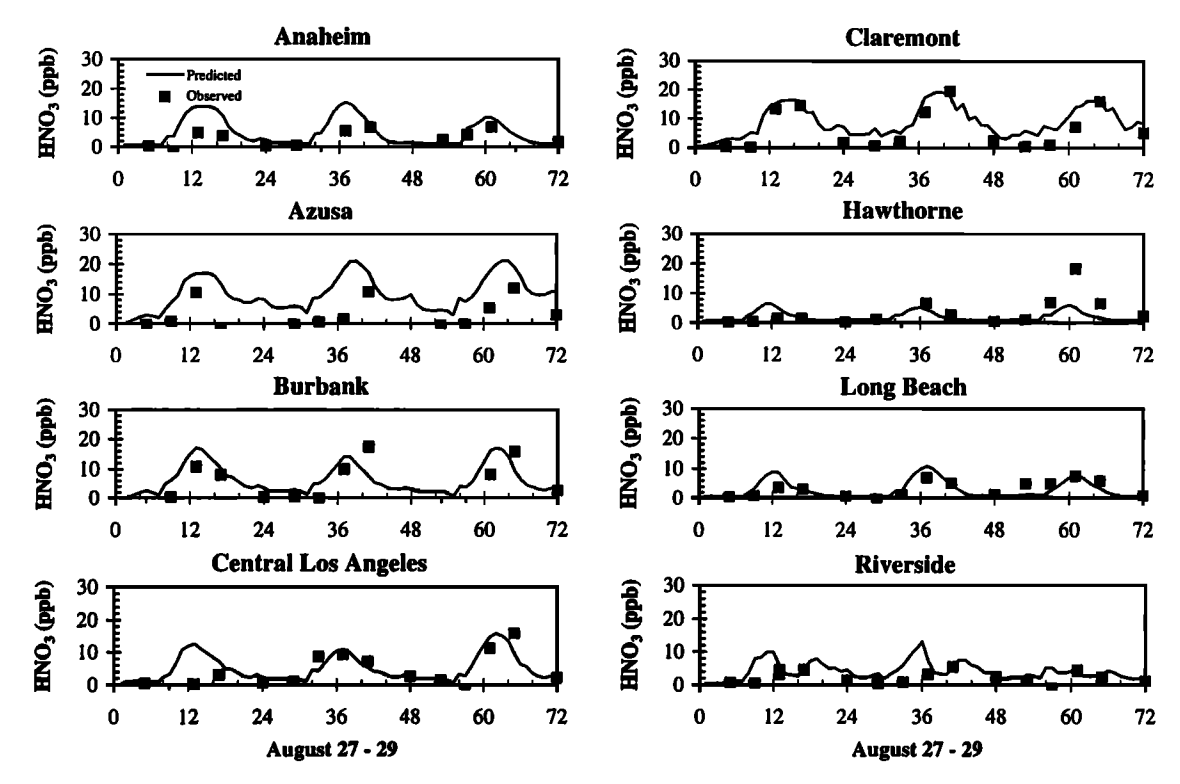


Figure 7. Time-series of predicted and observed gaseous nitric acid concentrations at various locations during August 27-29, 1987.

 m^{-3} which are considerably higher than the 12.7, 13.4, and 14.8 $\mu g \ m^{-3}$ measured on the 3 days. Note that the Teflon filter sampled PM_{10} nitrate concentrations were even lower than the $PM_{2.5}$ nitrate from the denuder difference method, suggesting that losses occurred during PM_{10} nitrate sampling by Teflon filters.

The maximum 24-hour means of nitrate occurred at Riverside for all 3 days. The predicted 48.0, 60.5, and 65.2 μ g m⁻³ of PM_{2.5} nitrate at Riverside are higher than the 39.1, 41.3, and 42.5 μ g m⁻³ measured on August 27, 28, and 29, respectively. The predicted maximum 24-hour mean PM₁₀ nitrate, at Riverside, 53.5, 68.5, and 71.2 μ g m⁻³, are to be compared with the 36.8, 40.1, and 42.9 μ g m⁻³ measured by Teflon filters.

Overprediction of PM nitrate is a result of overprediction of total nitrate. Total nitrate predicted by the current model is very close to that given by $Harley\ et\ al.$ [1993]. This behavior indicates that the gas-phase photochemistry may be producing too much HNO_3 . There are two pathways for production of HNO_3 : (1) NO_2 + OH and (2) N_2O_5 + H_2O . The second pathway contributes about a quarter of the total nitrate production.

7.2. Ammonium

Figure 6 shows patterns of predicted and observed PM_{2.5} ammonium at eight locations. Observations are based on Teflon filter samples plus the estimated volatilized ammonium. The volatilized ammonium is assumed to be in combination with nitrate and is determined by the difference between PM_{2.5} nitrate sampled by the denuder difference method and the Teflon filter method. Although the PM_{2.5} ammonium was also measured on an oxalic acid filter downstream of an oxalic acid coated glass tube denuder, the samples were contaminated when the denuder

became overloaded at Riverside due to the high ammonia concentrations [Hering et al., 1997]. At other locations the ammonium ion concentrations inferred by this method agreed with those measured by the denuder difference method.

Predicted 24-hour means of PM $_{2.5}$ ammonium averaged over the eight SCAQS observation stations are 6.4, 8.3, and 8.3 μ g m $^{-3}$ which agree well with the 6.5, 8.4, and 9.6 μ g m $^{-3}$ measured on August 27, 28, and 29, respectively. The predicted 24-hour means of PM $_{10}$ ammonium averaged over the eight SCAQS observation stations are 7.3, 8.9, and 8.9 μ g m $^{-3}$ which are higher than the 4.3,

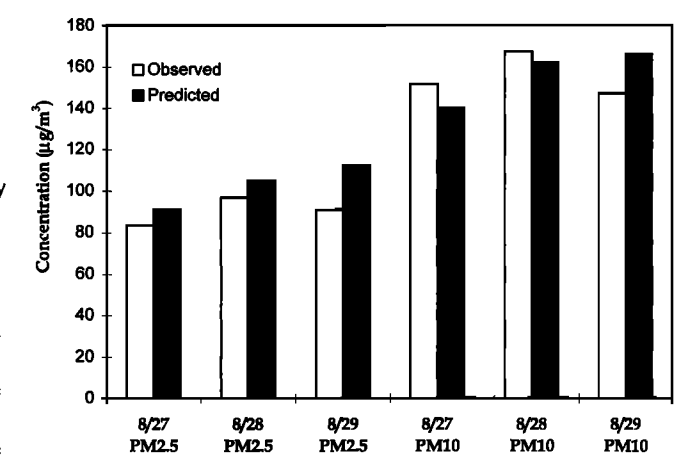


Figure 8. Predicted and observed maximum 24-hour-mean PM_{2.5} and PM₁₀ mass concentrations of the eight SCAQS monitoring stations during August 27-29, 1987. The maxima all occurred at Riverside.

Species	Mean Observed	Mean Predicted	Mean Bias	Mean Normalized Bias ,%	Mean Error	Mean Normalized Error, %
HNO ₃	12.7	18.0	5.3	56	7.1	67
NH ₃	3.3	1.5	-1.8	-33	2.3	79
$PM_{2.5}SO_4$	9.1	6.4	-2.7	-30	3.0	34
$PM_{2.5} NH_4$	8.4	8.3	-0.2	-1.0	2.3	29
$PM_{2.5} NO_3$	17.2	23.9	6.7	47	9.0	61
PM _{2.5} EC	3.0	3.8	0.8	35	1.3	50
PM _{2.5} OM	12.0	12.8	0.8	14	4.5	40
PM _{2.5} Mass	49.6	70.4	20.7	46	20.7	46

Table 7. Model Performance on 24-hour Mean Concentrations Averaged Over the Eight SCAQS Observation Stations on August 28, 1987

Units are in μ g m⁻³. The 24-hour mean of the measured concentrations is based on the five samples within each day. If some samples are missing, averages are performed only on the available samples, and the predicted concentrations are averaged for the same periods accordingly. Measured PM_{2.5}, NO₃⁻, and NH₄⁺ concentrations used are from the denuder samples that recover evaporated NO₃⁻ and NH₄⁺ during sampling while Teflon filter measurements were only available for the PM₁₀ samples. Thus the reported measured PM_{2.5} concentrations can be occasionally larger than the corresponding PM₁₀ concentrations. Mean bias is $D = (1/N) \sum_{i=1}^{N} (c_p(x_i, t) - c_o(x_i, t))$; Mean normalized bias is $D^* = (1/N) \sum_{i=1}^{N} (c_p(x_i, t) - c_o(x_i, t)) / (c_o(x_i, t))$; Mean error is $E = (1/N) \sum_{i=1}^{N} |c_p(x_i, t) - c_o(x_i, t)|$; Mean normalized error is $E^* = (1/N) \sum_{i=1}^{N} |c_p(x_i, t) - c_o(x_i, t)| / (c_o(x_i, t)) / (c_o(x_i, t))$; N is the number of 24-hour mean concentration prediction-observation pairs drawn from all monitoring stations for the day; c_p is the predicted 24-hour concentration at location x_i and date t; c_0 is the observed 24-hour concentration at monitoring station of monitoring station t.

5.7, and 8.1 μ g m⁻³ measured on the 3 days. Note that similar to nitrate the Teflon filter sampled PM₁₀ ammonium concentrations are also lower than the PM_{2.5} ammonium from the denuder method. Maximum 24-hour means of ammonium occurred at Riverside for all 3 days. Predicted maximum PM_{2.5} ammonium concentrations also agree very well with observations.

7.3. Nitric Acid

Predicted and observed time series HNO₃ are shown in Figure 7. Predicted 24-hour HNO₃ means averaged over the eight SCAQS observation stations are 6.3, 7.1, and 6.6 ppb, which exceed the 3.2, 5.0, and 5.9 ppb measured on August 27, 28, and 29, respectively. Overpredictions occurred at Azusa because of the timing differences of the peak values. Maximum 24-hour means of HNO₃ occurred at Claremont and Burbank. The predicted 9.4, 7.9, and 9.6 ppb of HNO₃ are comparable with the 7.4, 9.2, and 8.8 ppb measured on August 27, 28, and 29, respectively.

7.4. Sulfate

Predicted 24-hour means of PM_{2.5} sulfate averaged over the eight stations are 5.3, 6.4, and 6.3 μ g m⁻³ which are considerably lower than the 6.5, 9.1, and 13.7 μ g m⁻³ measured on August 27, 28, and 29, respectively. Predicted 24-hour means of PM₁₀ sulfate are 6.6, 7.8, and 7.8 μ g m⁻³, which are also lower than the 7.9, 11.0, and 16.4 μ g m⁻³ measured on the 3 days. Underprediction was most severe on the third day, when morning

fogs and low clouds penetrated farther into the coastal valleys, suggesting that most of the sulfate underprediction can be attributed to sulfate formed in the aqueous phase, a process that is not currently treated in the model.

7.5. PM Mass

The 24-hour means of PM mass at the station where the maximum occurred are shown in Figure 8. PM mass is overpredicted when PM $\rm NH_4NO_3$ is overpredicted. Maximum 24-hour means of PM mass all occurred at Riverside. The predicted 92.9, 107, and 113 μg m 3 of PM $_{25}$ mass at Riverside agree well with the 83.5, 96.8, and 90.6 μg m 3 measured on the 3 days. Predicted maximum PM $_{10}$ mass is 140, 164, and 167 μg m 3 , in proximity to the measured 152, 167, and 147 μg m 3 .

7.6. Summary of Performance Evaluation

The predicted 24-hour mean concentrations of the total $PM_{2.5}$ mass are above the observed values by an average of 15% during the entire 3-day episode focused on in this study. Similarly, the predicted 24-hour mean concentrations of the total PM_{10} mass are also above the observed data by an average of 7.5% during the entire episode. In particular, 24-hour mean nitrate $PM_{2.5}$ and PM_{10} concentrations are overpredicted by an average of 5.6 and 10.5 μg m⁻³, respectively. As discussed previously, this nitrate overprediction is the effect of excess HNO_3 produced by gasphase chemistry. Predictions of $PM_{2.5}$ ammonium 24-hour mean concentrations are almost identical to observations. During the

Species	Location	Maximum Observed	Maximum Predicted	Maximum in Domain ^a
HNO ₃	Burbank	23.3	20.0	40.3
NH ₃	Riverside	11.7	5.9	88.8
$PM_{2.5}SO_4$	Long Beach	11.4	12.9	19.1
$PM_{2.5} NH_4$	Riverside	15.5	17.5	21.0
$PM_{2.5} NO_3$	Riverside	41.3	60.5	72.9
PM _{2.5} EC	Azusa	5.6	5.4	7.2
$\mathrm{PM}_{2.5}\mathrm{OM}$	Azusa	17.9	16.3	24.5
PM _{2.5} Mass	Riverside	96.8	106.5	126

Table 8. Model Performance at the Monitoring Station at Which the Maximum 24-Hour Mean Concentration Was Observed on August 28, 1987

Units are in μ g m⁻³. The 24-hour mean of the measured concentrations is based on the five samples within each day. If some samples are missing, averages are performed only on the available samples, and the predicted concentrations are averaged for the same periods accordingly. Measured PM_{2.5} NO₃ and NH₄ concentrations used are from the denuder samples that recover evaporated NO₃ and NH₄ during sampling while Teflon filter measurements were only available for the PM₁₀ samples. Thus the reported measured PM_{2.5} concentrations can be occasionally larger than the corresponding PM₁₀ concentrations.

entire episode, $PM_{2.5}$ ammonium 24-hour average is underpredicted by 0.5 μg m⁻³. PM_{10} ammonium 24-hour mean concentrations are overpredicted by 2.3 μg m⁻³ during the entire episode.

8. Conclusions

We have developed a three-dimensional size-resolved and chemically resolved aerosol model that includes advection, turbulent diffusion, condensation/evaporation, nucleation, emissions, and dry deposition. For condensation/evaporation of volatile inorganic species a new thermodynamic model SCAPE2, which has a comprehensive treatment of gas-aerosol equilibrium is incorporated. The aerosol model has been coupled with the three-dimensional gas-phase photochemical CIT model and has been applied to the August 27-29, 1987 episode in the South Coast Air Basin of California. Simulations have been compared systematically against available observations.

Acknowledgment. This work was supported by the Electric Power Research Institute (EPRI), the IBM Environmental Research Program, and the General Motors Corporation. Any opinions, findings, and conclusions or recommendations expressed in this material are those of the authors and do not necessarily reflect the views of EPRI and/or the IBM Corporation.

References

Anthes, R. A., E. Y. Hsie, and Y. H. Kuo, Description of the Penn State/NCAR mesoscale model version 4 (MM4), NCAR Tech. Note NCAR/TN-282+STR, Nat. Cent. for Atmos. Res., Boulder, Colo., 1987.

- Binkowski, F. S., and U. Shankar, The regional particulate matter model, 1, Model description and preliminary results, J. Geophys. Res., 100, 26,191-26,209, 1995.
- Carter, W. P. L., A detailed mechanism for the gas-phase atmospheric reactions of organic compounds, Atmos. Environ., Part A, 24, 481-518, 1990.
- Cass, G. R., and S. Gharib, Ammonia emissions in the South Coast Air Basin 1982, Open File Rep. 84-2, Environ. Qual. Lab., Calif. Inst. of Technol., Pasadena, Calif., 1984.
- Chang, J. S., et al., The regional acid deposition model and engineering model, NAPAP Rep. 4, Nat. Acid Precip. Assess. Program, Washington, D. C., 1991.
- Countess, R. J., Southern California Air Quality Study sampler chemistry, final rep. under contract A5-186-32, to Calif. Air Resour. Board, Sacramento, 1989.
- Dhaniyala, S., and A. S. Wexler, Numerical schemes to model condensation and evaporation of aerosols, Atmos. Environ., 30, 919-928, 1996.
- Gelbard, F., and J. H. Seinfeld, Simulation of multicomponent aerosol dynamics, J. Colloid Interface Sci., 78, 541-556, 1980.
- Gelbard, F., Y. Tambour, and J. H. Seinfeld, Sectional representation for simulating aerosol dynamics, J. Colloid Interface Sci., 76, 485-501, 1980.
- Goodin, W. R., G. J. McRae, and J. H. Seinfeld, A comparison of interpolation methods for sparse data: Application to wind and concentration fields, J. Appl. Meteorol., 18, 761-771, 1979.
- Goodin, W. R., G. J. McRae, and J. H. Seinfeld, An objective analysis technique for constructing three-dimensional, urban-scale wind fields, J. Appl. Meteorol., 19, 98-108, 1980.
- Harley, R. A., A. F. Russell, G. J. McRae, G. R. Cass, and J. H. Seinfeld, Photochemical modeling of the Southern California Air Quality Study, Environ. Sci. Technol., 27, 378-388, 1993.
- Hering, S., A. Eldering, and J. H. Seinfeld, Bimodal character of accumulation mode aerosol mass distributions in southern California, *Atmos. Environ.*, 31, 1-11, 1997.
- Jacobson, M.Z., Development and application of a new air pollution modeling system, III, Aerosol-phase simulations, Atmos. Environ., 31, 587-608, 1997.
- John, W., S. M. Wall, J. L. Ondo, and W. Winklmayr, Acidic aerosol size distributions during SCAQS, Compilation of data tables and graphs, Calif. Air Resour. Board, Sacramento, 1989.

^a Maximum 24-hour mean concentration predicted anywhere in entire domain.

- Kim, Y. P., and J. H. Seinfeld, Atmospheric gas-aerosol equilibrium, III, Thermodynamics of crustal elements Ca²⁺, K⁺, and Mg²⁺, Aerosol Sci. Technol., 22, 93-110, 1995.
- Kim, Y. P., J. H. Seinfeld, and P. Saxena, Atmospheric gas-aerosol equilibrium, I, Thermodynamic model, Aerosol Sci. Technol., 19, 157-181, 1993a.
- Kim, Y. P., J. H. Seinfeld, and P. Saxena, Atmospheric gas-aerosol equilibrium, II, Analysis of common approximations and activity coefficient calculation methods, *Aerosol Sci. Technol.*, 19, 182-198, 1993b.
- Lurmann, F. W., W. P. L. Carter, and L. A. Coyner, A surrogate species chemical reaction mechanism for urban-scale air quality simulation models, Vol. I and II., Rep. to the U.S. Environ. Prot. Agency, contract 68-02-4104, ERT Inc., Newbury Park, Calif., and Statewide Air Poll. Res. Cent., Univ. of Calif., Riverside, 1987.
- Lurmann, F. W., A. S. Wexler, S. N. Pandis, S. Musarra, N. Kumar, and J. H. Seinfeld, Modelling urban and regional aerosols, II, Application to California's South Coast Air Basin, Atmos. Environ., 31, 2695-2715, 1997.
- McRae, G. J., and J. H. Seinfeld, Development of a second-generation mathematical model for urban air pollution, 2, Evaluation of model performance, Atmos. Environ., 17, 501-522, 1983.
- McRae, G. J., W. R. Goodin, and J. H. Seinfeld, Development of a second-generation mathematical model for urban air pollution, 1, Model formulation, Atmos. Environ., 16, 679-696, 1982.
- Meng, Z., and J. H. Seinfeld, Timescales to achieve atmospheric gasaerosol equilibrium for volatile species, Atmos. Environ., 30, 2889-2900, 1996.
- Meng, Z., J. H. Seinfeld, P. Saxena, and Y. P. Kim, Atmospheric gasaerosol equilibrium, IV, Thermodynamics of carbonates, Aerosol Sci. Technol., 23, 131-154, 1995a.
- Meng, Z., J. H. Seinfeld, and P. Saxena, Gas/aerosol distribution of formic and acetic acids, *Aerosol Sci. Technol.*, 23, 561-578, 1995b.
- Odum, J. R., T. Hoffmann, F. Bowman, D. Collins, R. C. Flagan, and J. H. Seinfeld, Gas/particle partitioning and secondary organic aerosol yields, *Environ. Sci. Technol.*, 30, 2580-2585, 1996.
- Odum, J. R., T. P. W. Jungkamp, R. J. Griffin, R. C. Flagan, and J. H. Seinfeld, The atmospheric aerosol-forming potential of whole gasoline vapor, Science, 276, 96-99, 1997.
- Pandis, S. N., R. A. Harley, G. R. Cass, and J. H. Seinfeld, Secondary organic aerosol formation and transport, *Atmos. Environ.*, 26, 2269-2282, 1992a.
- Pandis, S. N., J. H. Seinfeld, and C. Pilinis, Heterogeneous sulfate production in an urban fog, Atmos. Environ., Part A, 26, 2509-2522, 1992b.
- Pandis, S. N., A. S. Wexler, and J. H. Seinfeld, Secondary organic aerosol formation and transport, 2, Predicting the ambient secondary organic aerosol-size distribution, Atmos. Environ., 27, 2403-2416, 1993.
- Pilinis, C., Derivation and numerical solution of the species mass distribution equations for multicomponent particulate systems, *Atmos. Environ.*, *Part A*, 24, 1923-1928, 1990.
- Pilinis, C., and J. H. Seinfeld, Continued development of a general equilibrium model for inorganic multicomponent atmospheric aerosols, *Atmos. Environ.*, 21, 2453-2466, 1987.
- Pilinis, C., and J. H. Seinfeld, Development and evaluation of an Eulerian photochemical gas-aerosol model, Atmos. Environ., 22, 1985-2001, 1988.
- Robinson, R. A., and R. J. Stokes, *Electrolyte Solutions*, 2nd ed., Butterworths, London, 1965.
- Russell, A. G., K. F. McCue, and G. R. Cass, Mathematical-modeling of the formation of nitrogen-containing air pollutants, 1, Evaluation of an Eulerian photochemical model, *Environ. Sci. Technol.*, 22, 263-270, 1988.
- Russell, A. G., D. A. Winner, R. A. Harley, K. F. McCue, and G. R. Cass, Mathematical modeling and control of the dry deposition flux of

- nitrogen-containing air pollutants, Environ. Sci. Technol., 27, 2772-2782, 1993.
- Saxena, P., A. B. Hudischewskyj, C. Seigneur, and J. H. Seinfeld, A comparative study of equilibrium approaches to the chemical characterization of secondary aerosols, *Atmos. Environ.*, 20, 1471-1483, 1986.
- Solomon, P. A., T. Fall, S. M. Larson, P. Lin, F. Vasquez, and G. R. Cass, Acquisition of acid and aerosol concentration data for use in dry deposition studies in the South Coast Air Basin, I, report, contract A4-144-32, Calif. Air Resour. Board, Sacramento, 1980.
- Stockwell, W. R., D. Middleton, J. S. Chang, and X. Tang, The second-generation Regional Acid Deposition Model chemical mechanism for regional air quality modeling, J. Geophys. Res., 95, 16,343-16,367, 1990.
- Systems Applications International (SAI), User's guide for the urban airshed model, I, Rep. SYSAPP-90/018a, Syst. Appl. Int., San Rafael, Calif., 1990a.
- Systems Applications International (SAI), User's guide for the urban airshed model, II, preprocessors and postprocessors for the UAM modeling system, *Rep. SYSAPP-90/018b*, Syst. Appl. Int., San Rafael, Calif., 1990b.
- Systems Applications International (SAI), User's guide for the urban airshed model, III, the diagnostic wind model, Rep. SYSAPP-90/018c, Syst. Appl. Int., San Rafael, Calif., 1990c.
- Systems Applications International (SAI), User's guide for the urban airshed model, IV, the emissions preprocessor system, Rep. SYSAPP-90/018d, Syst. Appl. Int., San Rafael, Calif., 1990d.
- Systems Applications International (SAI), User's guide for the urban airshed model, Vol. V: description and operation of the ROM-UAM interface program system, *Rep. SYSAPP-90/018e*, Syst. Appl. Int., San Rafael, Calif., 1990e.
- Wagner, K. K., and P. D. Allen, SCAQS emissions inventory for August 27-29, 1987 (Tape ARA714), Tech. Support Div., Calif. Air Resour. Board, Sacramento, 1990.
- Wexler, A. S., F. W. Lurmann, and J. H. Seinfeld, Modeling urban and regional aerosols, I, Model development, Atmos. Environ., 28, 531-546, 1994.
- Wexler, A. S., and J. H. Seinfeld, Second-generation inorganic aerosol model, Atmos. Environ., Part A, 25, 579-591, 1991.
- Wexler, A. S., and J. H. Seinfeld, The distribution of ammonium salts among a size and composition dispersed aerosol, *Atmos. Environ.*, *Part A*, 24, 1231-1246, 1990.
- Winklmayr W., H. C. Wang, and W. John, Adaptation of the Twomey algorithm to the inversion of cascade impactor data, Aerosol Sci. Technol., 13, 322-331, 1990.
- Yotter, E. E., and D. L. Wade, Development of a gridded motor vehicle emission inventory for the Southern California Air Quality Study, Paper presented at the 82nd annual meeting of the Air and Waste Management Association, Anaheim, Calif., 1989.
- D. Dabdub, Department of Mechanical and Aerospace Engineering, University of California, Irvine, Irvine, CA 92697-3975. (e-mail: dabdub@masaya.eng.uci.edu)
- Z. Meng, Department of Environmental Engineering Science, California Institute of Technology, Pasadena, CA 91125. (e-mail: rmeng@fx.com)
- J. H. Seinfeld, Division of Engineering and Applied Science and Department of Chemical Engineering, California Institute of Technology, Pasadena, CA 91125. (e-mail: john_seinfeld@starbasel.caltech.edu)

(Received April 4, 1997; revised September 15, 1997; accepted September 17, 1997.)